AGU PUBLICATIONS

Geophysical Research Letters

RESEARCH LETTER

10.1002/2014GL059595

Key Points:
- Three-dimensional numerical models featuring both plate tectonics and supercontinent cycles
- Modeled supercontinent cycles are not regular but underlie strong fluctuations
- Average assembly and breakup times are controlled by the strength of plates

Correspondence to:
T. Rolf,
Tobias.Rolf@geo.uio.no

Citation:
Rolf, T., N. Coltice, and P. J. Tackley (2014), Statistical cyclicity of the supercontinent cycle, *Geophys. Res. Lett.*, *41*, doi:10.1002/2014GL059595.

Received 11 FEB 2014
Accepted 21 MAR 2014
Accepted article online 25 MAR 2014

Statistical cyclicity of the supercontinent cycle

T. Rolf[1,2,3], N. Coltice[4,5], and P. J. Tackley[1]

[1]Institute of Geophysics, ETH Zurich, Zurich, Switzerland, [2]School of Geosciences, Monash University, Clayton, Victoria, Australia, [3]Now at Centre for Earth Evolution and Dynamics, University of Oslo, Oslo, Norway, [4]Laboratoire de Géologie, Université Claude Bernard Lyon 1, Villeurbanne, France, [5]Institut Universitaire de France, Paris, France

Abstract Supercontinents like Pangea impose a first-order control on Earth's evolution as they modulate global heat loss, sea level, climate, and biodiversity. In a traditional view, supercontinents form and break up in a regular, perhaps periodic, manner in a cycle lasting several 100 Myr as reflected in the assembly times of Earth's major continental aggregations: Columbia, Rodinia, and Pangea. However, modern views of the supercontinent cycle propose a more irregular evolution on the basis of an improved understanding of the Precambrian geologic record. Here we use fully dynamic spherical mantle convection models featuring plate-like behavior and continental drift to investigate supercontinent formation and breakup. We further dismiss the concept of regularity but suggest a statistical cyclicity in which the supercontinent cycle may have a characteristic period imposed by mantle and lithosphere properties, but this is hidden in immense fluctuations between different cycles that arise from the chaotic nature of mantle flow.

1. Introduction

Alfred Wegener first postulated the assembly of Earth's continents into a single landmass, Pangea. It started to break up ~180 Myr ago after which its fragments have drifted into their present dispersed configuration. The supercontinent cycle describes the assembly of Earth's continents and their subsequent breakup and dispersal and is of fundamental importance for global sea level changes [*Worsley et al.*, 1984], atmospheric evolution [*Campbell and Allen*, 2008] and biodiversity [*Rogers and Santosh*, 2004].

However, since its first proposal [e.g., *Worsley et al.*, 1984] the supercontinent cycle has remained controversial. Numerous indications for the existence of supercontinent assemblies have been detected in the geologic record, e.g., in the abundance of passive margins [*Bradley*, 2011]. Clearly, detecting and dating these assemblies in a fragmentary record consisting of only preserved rocks [*Roberts*, 2012] is complicated. Thus, only the formation and breakup of Pangea is well documented, while existence and dynamics of Precambrian supercontinents remain debated. Nevertheless, several data records, e.g., the age distributions of detrital zircons [*Campbell and Allen*, 2008] and granites [*Condie et al.*, 2009], suggest a pronounced cyclicity of continental assembly with a period of 700–800 Myr as reflected by the proposed formation times of supercontinents Kenorland (~2600 Ma), Columbia (~1800 Ma), Rodinia (~1100 Ma), and Pangea (~400 Ma) [*Rogers and Santosh*, 2003].

If supercontinent formation and breakup is one of Earth's major tectonic processes, it likely has broad implications for the geologic and atmospheric evolution. Thus, understanding its regularity (or irregularity) may help to interpret the Precambrian geologic record and Earth's long-term evolution. Consequently, this study aims to shed more light on the dynamic evolution of supercontinents and its timescales.

Starting with *Gurnis* [1988] numerical modeling has often been used to study supercontinent dynamics, with some recent works reporting surprisingly uniform supercontinent timescales [e.g., *Phillips and Bunge*, 2007]. However, these studies often neglected the interplay of continental and oceanic plates or were in 2-D. Global dynamic 3-D models including both types of Earth's lithosphere are still rare and have to date either focused on supercontinent assembly only [*Zhang et al.*, 2009] or have not generated more than one supercontinent cycle [*Yoshida and Santosh*, 2014], which does not allow evaluation of the diversity of supercontinent dynamics and fluctuations in the associated timescales.

Here we use fully dynamic 2-D and 3-D numerical models of mantle convection that show the cyclic alternation of assembled and dispersed continents in the framework of plate tectonics for the first time. In contrast to previous models [*Gurnis*, 1988; *Lenardic et al.*, 2000; *Phillips and Bunge*, 2007], our models combine

Table 1. Reference Parameters That are Used to Convert Nondimensional Model Parameters to Dimensional Values[a]

Symbol	Definition	Value
α_0	Thermal expansivity	3×10^{-5} K^{-1}
g_0	Gravitational acceleration	10 m s^{-2}
D_0	Mantle thickness	2.89×10^6 m
ΔT	Temperature drop over lithosphere	1300 K
T_S	Surface temperature	300 K
ρ_0	Normal mantle density	3300 kg m^{-3}
k_0	Thermal conductivity	3.15 W m^{-1} K^{-1}
κ_0	Thermal diffusivity	1×10^{-6} m^2 s^{-1}
η_0	Viscosity (observed at $T = 1$)	3.1×10^{22} Pa s
τ_E	Transit time of Earth's mantle	8.5×10^7 yr

[a]In the transit time framework (see text), dimensional temperatures are obtained by $T_{(K)} = T_S + T\Delta T$. Viscosities are scaled by $\eta_{(Pa\,s)} = \eta_0\eta$, depth scales with $d_{(m)} = D_0 d$, stresses with $\sigma_{(Pa)} = \sigma\eta_0\tau/\tau_E$, yield stress gradients with $\sigma'_{(Pa/m)} = \sigma'\eta_0\tau/D_0\tau_E$ and the internal heating rate with $H_{(W/kg)} = Hk_0\Delta T\tau/\kappa_0\rho_0\tau_E$, where $\tau = D/v_{RMS}$ is the time-averaged nondimensional transit time observed for the accordant yield strength, as given by the ratio of nondimensional mantle thickness $D = 1$ and the root-mean-square (RMS) velocity of the whole mantle.

continental drift, oceanic plates, and Earth-like seafloor spreading in 3-D and illustrate tectonic evolution over significantly more supercontinent cycles than in previous studies [*Yoshida and Santosh*, 2014]. We compile synthetic databases of continental assembly and dispersal times in order to discuss supercontinent timescales statistically. We focus on the regularity of these timescales and how they are linked to the large-scale mantle flow.

2. Methods

For investigating the timescales of supercontinent assembly and dispersal, we compute numerical solutions of spherical mantle convection featuring self-consistently generated plate-like behavior and continental drift [*Rolf et al.*, 2012] that have been shown to reproduce Earth's seafloor age distribution reasonably well [*Coltice et al.*, 2012]. Following, e.g., *Lenardic et al.* [2000], continents consist of two different materials, namely a strong interior ($k = 1$, representing an Archean craton) surrounded by weaker material ($k = 2$). The latter facilitates continental rifting [*Murphy et al.*, 2006] and improves the long-term stability of the cratonic interior [*Lenardic et al.*, 2000].

Both continental materials are parametrized by continuous fields ($0 \le C_k \le 1$), which are tracked in time by using the tracer-ratio method [*Tackley and King*, 2003]: $C_1 = 1$ represents pure Archean craton, $C_2 = 1$ pure weak material, and $C_1 = C_2 = 0$ pure normal mantle. Continental material differs from the latter in terms of density and rheology. The density contrast is specified by the buoyancy ratio $R_k = \Delta\rho_k/\rho_0\alpha_0\Delta T$, i.e., the ratio of the density difference $\Delta\rho_k$ between material k and normal mantle to the thermal density variation $\rho_0\alpha_0\Delta T$. With the definitions and values given in Table 1, the applied ratios $R_1 = R_2 = -0.4$ correspond to a density contrast of about -50 kg m^{-3}.

The rheological contrast between different materials is controlled by two parameters. First, a viscosity contrast $\Delta\eta_{C_k} = \eta_T(T, C_k = 1)/\eta_T(T, C_1 = C_2 = 0)$ is applied to define the viscosity ratio of pure material k and normal mantle. Here the temperature-dependent viscosity η_T is calculated by an Arrhenius law

$$\eta_T = \exp\left[\frac{E_A}{T+1} - \frac{E_A}{2}\right] \cdot \prod_{k=1}^{k=2} \exp\left[\ln(\Delta\eta_{C_k})C_k\right]. \quad (1)$$

The activation parameter is set to $E_A = 23.03$, which leads to a thermal viscosity variation of 10^5 in the interval $0 \le T \le 1$. $\Delta\eta_{C_1}$ and $\Delta\eta_{C_2}$ are set to 100 and 0.1.

The second rheological control parameter is the yield stress ratio $\Delta\sigma_{Y_k} = \sigma_Y(d, C_k = 1)/\sigma_Y(d, C_1 = C_2 = 0)$. Here the yield stress σ_Y is the maximum stress material can sustain without deforming plastically and is assumed to increase linearly with increasing depth d,

$$\sigma_Y = \left(\sigma_0 + d \cdot \sigma'_Y\right) \cdot \prod_{k=1}^{k=2} \exp\left[\ln(\Delta\sigma_{Y_k})C_k\right], \quad (2)$$

where $\sigma_0 = \sigma_Y(d = 0, C_1 = C_2 = 0)$ is the surface value for the reference material and σ'_Y is the depth gradient. All yielding parameters except for σ_0 are kept constant for simplicity: $\Delta\sigma_{Y_1} = \Delta\sigma_{Y_2} = 10$ and $\sigma'_Y = 2 \times 10^5$ (~3 MPa/km, see Table 1). The yield stress limits the viscosity by $\eta_Y = \sigma_Y/2\dot{\epsilon}$, where $\dot{\epsilon}$ is the second invariant of the strain-rate tensor, such that the effective viscosity is given by $\eta = \left[1/\eta_T + 1/\eta_Y\right]^{-1}$.

This rheology is sufficient to generate large tectonic plates separated by narrow weak plate boundaries, but plate-like behavior is improved by a parametrized weak asthenosphere. A viscosity reduction by a factor of 0.1 is applied, if material becomes hotter than its solidus, which is given by an empirical fit to experimental data [see *Xie and Tackley*, 2004, and references therein].

2.1. Analysis of Continental Drift

We designed a set of calculations with the minimum complexity needed for analyzing supercontinent timescales: only two continental blocks are considered, such that the continental configuration is always either assembled or dispersed and the lifetime of a certain configuration can easily be estimated. In 2-D, this estimation is automatized by tracking the angular distance γ between the centroids of the two continents. Due to the presence of mobile weak zones, continents cannot be considered as quasi-rigid here (as in *Rolf et al.* [2012]) and continental deformation has to be taken into account by applying the criterion

$$\gamma_{\mathrm{norm}}(t) \leq \gamma_{\mathrm{crit}} \quad \Leftrightarrow \quad \text{Continents assembled.} \tag{3}$$

Here $\gamma_{\mathrm{norm}} = \gamma/(r_1(t) + r_2(t))$ is the angular distance between continents 1 and 2 normalized with the sum of both (angular) continental radii, which are initially $r_1(0) = r_2(0) = 0.2\pi$, such that each continent covers ~20% of the surface (= 2π, if the spherical annulus is treated like a thin cylinder for this purpose). The time-dependent radii $r_k(t)$ can be estimated from the integrated area covered by continent k at time t. $\gamma_{\mathrm{crit}} = 1.04$–$1.07$ is an empirical threshold derived from comparison with visualizations of the compositional fields. Criterion (3) fully characterizes the configuration with only two continents. Transitions between an assembled and a dispersed configuration (or vice versa) mark supercontinent breakup (or collision) and thus determine the timescales of interest.

In the 3-D calculations, however, these timescales are estimated from visualizations only as we used continents with irregular and particularly asymmetric shape in order to avoid prescribed symmetries, such that criterion (3) becomes invalid in 3-D. The graphical estimation has some uncertainty, because breakup and collision are not instantaneous processes (as in 2-D), but will start earlier in one region of the continent than in another. However, we are confident that the uncertainty does not exceed 10–20 Myr, considerably smaller than the effects discussed below.

2.2. Numerical Simulations

For this study we performed a large suite of calculations in a spherical annulus (2-D) or a spherical shell (3-D). In all cases, convective vigor is reduced compared to Earth's mantle for computational reasons and the Rayleigh number for purely internal heating is $Ra_H = 2.05 \times 10^7$ based on an internal heating rate of $H = 20.5$ (~3.5×10^{-11} W kg^{-1}, see Table 1), a factor of ~5 higher than in the present-day Earth, as required to keep the nondimensional temperature drop across the surface boundary layer close to 1 (see Figure 1d). The resulting Ra_H is ~2 orders of magnitude smaller than Earth's [*Turcotte and Schubert*, 2002] such that one reference parameter has to deviate from its Earth-like value. Here this is the reference viscosity η_0 (see Table 1).

The lower Ra_H necessitates that the model continent thickness ($d_C = 0.15 \sim 430$ km) be increased relative to Earth's in order to maintain a similar continental to oceanic lithosphere thickness ratio. Finally, lower convective vigor causes a discrepancy between computed model time t (in nondimensional diffusion times) and geological time, which is accounted for by scaling the models' transit time τ to that of the present-day Earth's mantle τ_E, such that $t(\mathrm{Myr}) = t \cdot \tau_E/\tau$ (see Table 1), while keeping in mind that the present-day value is not necessarily a characteristic of Earth's long-term evolution, for which the transit time is mostly unknown.

As we aim to characterize the timescales and their fluctuations of typical supercontinent cycles, secular cooling of the mantle is neglected here ($H \neq f(t)$) in order to isolate the intrinsic fluctuations from those arising from Earth's long-term cooling history.

3. Results

An example of modeled continental drift is presented in Figure 1. Initially, the two continents are assembled in the Northern Hemisphere (Figure 1a), then split apart (Figure 1b), and reassemble in the Southern Hemisphere some 100 Myr after the breakup (Figure 1c). This motion is typical for the presented simulations

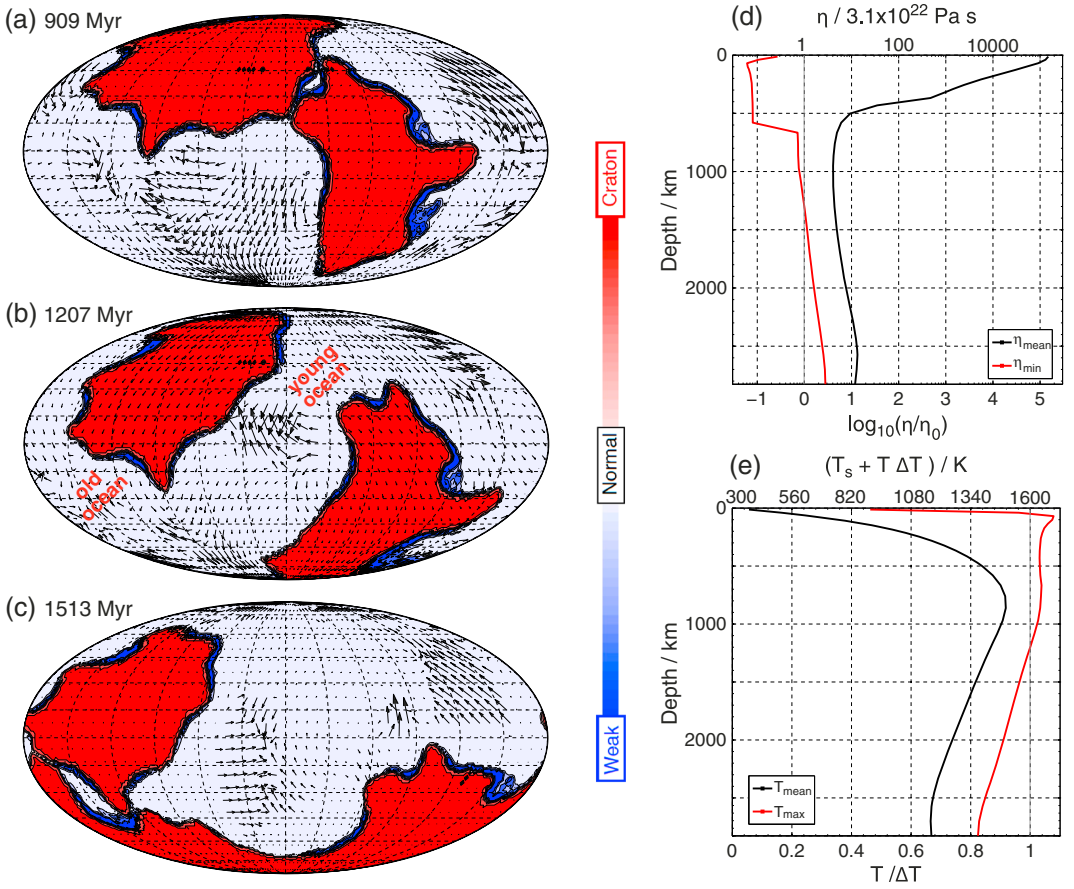

Figure 1. Example of a supercontinent cycle with $\sigma_0 = 10,000$ (~413 MPa). Shown are material compositions at the surface as defined in the color bar: (a) Old supercontinent, (b) Dispersal, and (c) New supercontinent. (d) Time-averaged radial profile of average and minimum viscosity. (e) As Figure 1d, but for maximum and average temperature. See Table 1 for dimensionalization of temperature, viscosity, and stress.

reflecting the extroversion type of supercontinent formation [*Murphy and Nance*, 2003] during which the old, exterior ocean is recycled rather than the younger, interior ocean.

The alternation of assembled and dispersed phases is more striking when considering long-term evolution of continental configuration (Figure 2). For instance, in the case discussed above (see Figure 2b), six completed supercontinent cycles with an average duration of 640 ± 105 Myr occur within a timespan of ~4 Gyr. This is very similar to the timescales suggested for Earth's supercontinent cycle [*Rogers and Santosh*, 2003; *Meert*, 2012] and shows that several almost periodic assembly and breakup events can occur. However, we calculated the evolution for 50 3-D cases (~10 cases, which only differ in the initial condition of the thermal field, for five different values of the yield parameter σ_0) and did not find this regularity to be a characteristic feature. Some cyclic behavior is observed in most cases, however, the length of assembled and dispersed intervals may vary significantly for given σ_0. Furthermore, these timescales are dependent on the value of σ_0. For a large yield parameter, a proxy for strong plates, supercontinent breakup is impeded and the period of continental assembly t_A is elongated (Figure 2d). On the contrary, weaker oceanic plates (small σ_0) favor much longer periods (t_D) during which both continents remain separated (Figure 2a).

As the timescales of assembly and dispersal vary significantly even for a given lithospheric strength, it is difficult to characterize these timescales and their fluctuations as well as their dependence on plate strength with such a small number of supercontinent cycles as shown in Figure 2. Thus, we gathered databases containing 100s of assembly and dispersal events, implementing corresponding 2-D simulations in a spherical annulus (5 × 35 calculations with integration times of >10 Gyr). Obviously, these models cannot account for 3-D features like continental shape and toroidal flow, but major similarities can be expected and performing the same analysis in 3-D is well beyond our computational resources.

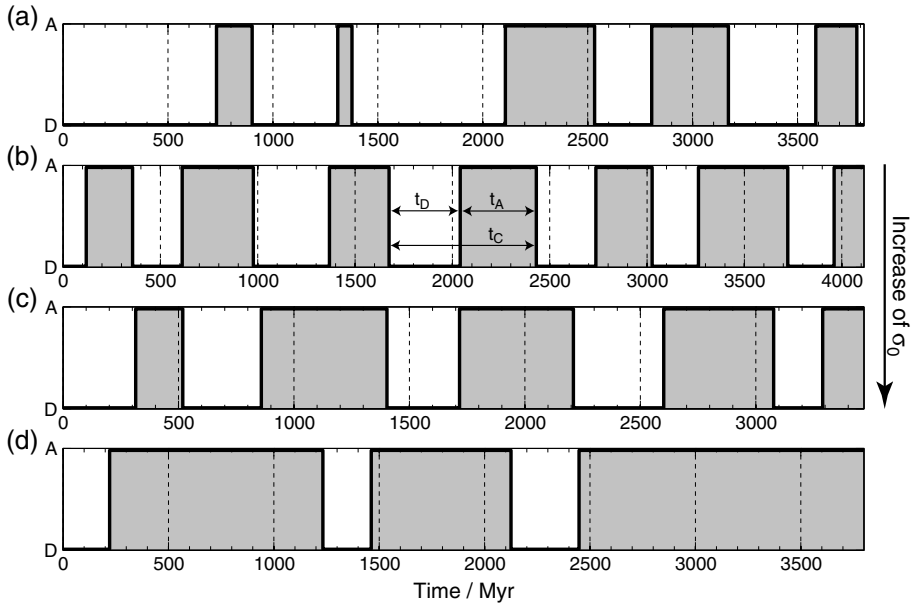

Figure 2. Time evolution of continental configurations: assembled *A* or dispersed *D*. Panels show representative examples of calculations with different yield parameter σ_0: (a) 5000 (~237 MPa), (b) 10,000 (~413 MPa), (c) 15,000 (~570 MPa), (d) 20,000 (~702 MPa). Arrows labeled with t_A, t_D, and t_C illustrate supercontinent timescales as used in subsequent figures.

Using these databases, supercontinent timescales and their fluctuations can be analyzed statistically. As an example, the results for $\sigma_0 = 10,000$ (~413 MPa) are shown in Figure 3. Based on 466 detected supercontinents, the timescale of supercontinent assembly t_A is almost symmetrically distributed (Figure 3a). Mean and median are similar and the standard deviation is moderate (~40%), which indicates a certain regularity of supercontinent breakup upon which fluctuations arising from time-dependent mantle flow are superimposed.

In contrast, the dispersed period of the supercontinent cycle (t_D) is described by a strongly skewed distribution with a long tail (Figure 3b), indicating that dispersed (present-day like) configurations can be maintained for up to 2 Gyr before a new supercontinent may form. This is much longer than suggested for Earth's history, but it may be explained by the higher degrees of freedom of continental drift during this dispersed phase [*Gurnis*, 1988].

In this case, only ~27% of modeled supercontinent cycles have a duration of 750 ± 100 Myr (Figure 3c), the Earth's timescale cycle recently inferred by *Meert* [2012]. The exact percentage depends on the yield

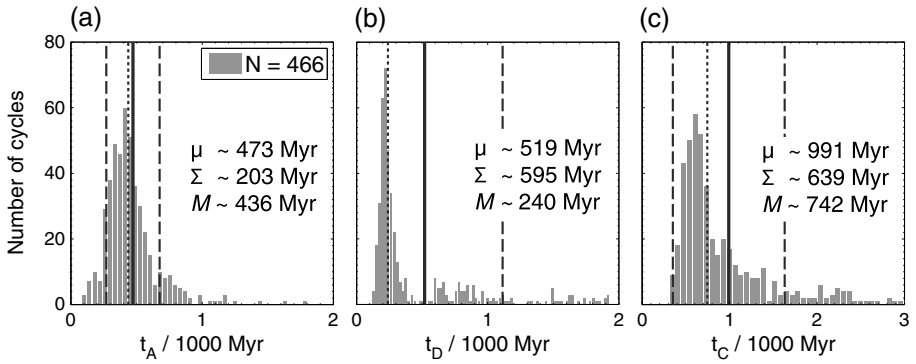

Figure 3. Timescale statistics for the 2-D calculations with $\sigma_0 = 10,000$ (~ 413 MPa). (a) Assembled period t_A, (b) dispersed period t_D, and (c) duration of a supercontinent cycle t_C. μ, Σ, and *M* denote mean value, standard deviation, and median as highlighted by the bold, dashed, and dotted lines, respectively. Histograms are based on $N = 466$ data points.

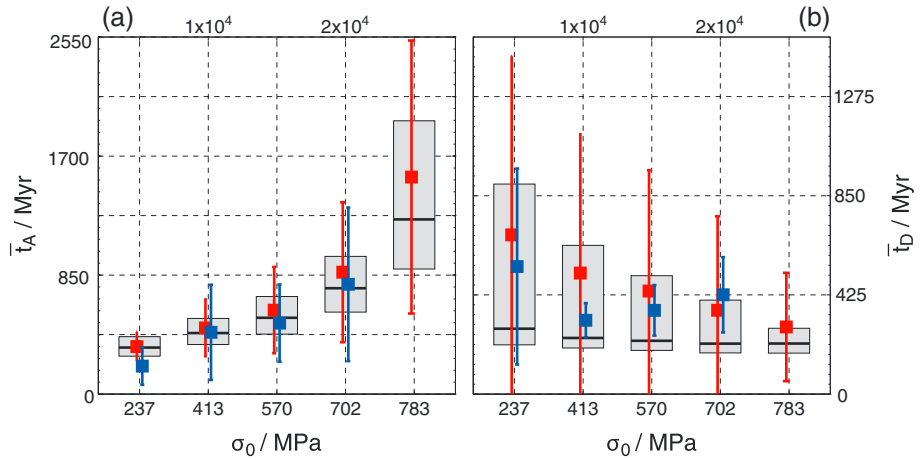

Figure 4. Averaged supercontinent timescales as a function of σ_0: (a) $\bar{t}_A$ and (b) $\bar{t}_D$. Red data points indicate mean ± standard deviation in the 2-D calculations (N = 408/466/491/385/254), blue data points display the corresponding 3-D results (N = 18/42/26/15/0). Grey boxes contain 50% of all 2-D data points and are bounded by the first and third quartile. The difference between median (black line) and mean is a measure for the skewness of the corresponding distribution of timescales. Note that the dimensional stress axis is somewhat nonlinear, because the scaling constant τ decreases with increasing σ_0.

parameter, but does not exceed the above value in the investigated cases, such that the majority of modeled cycles do not fall in the proposed range, which we note is only constrained by a very few supercontinents.

Nevertheless, a clear link between the timescales of assembly and dispersal and the properties of the plate-mantle system as discussed earlier (see Figure 2) is evident in the statistics. We calculated the average lifetime $\bar{t}_A$ of a supercontinent and the average duration of dispersed continent configurations $\bar{t}_D$ from the statistical distributions: these characteristic timescales are modulated by the strength of the lithosphere and vary by a factor of ~2–3 over the strength range investigated here (Figure 4). As expected, assembly prevails for a longer period the stronger the lithosphere is, because higher stresses have to be generated from mantle flow in order to overcome the lithospheric strength and enforce breakup (Figure 4a). This effect is observed in both 2-D and 3-D calculations with a reasonable match although the 3-D database is small and consequently more affected by the intrinsic fluctuations between different cycles, as discussed earlier. For the largest yield strength, breakup is generally difficult to achieve, which results in a more skewed distribution of t_A (not shown) and an enormous increase in the characteristic assembly timescale or even the complete lack of breakup events (in 3-D). This may indicate that the upper yield stress limit for which plate-like behavior can be observed is approached [see *Rolf and Tackley*, 2011].

Perhaps more surprisingly, the characteristic dispersal period $\bar{t}_D$ shows the opposite trend and decreases for stronger lithosphere (Figure 4b). A possible explanation is given by the effect of lithospheric strength on the wavelength of mantle flow. As reported previously [*Zhong et al.*, 2007; *Yoshida*, 2008], we observe enhanced long-wavelength flow for stronger lithosphere, which leads to few, but large tectonic plates and thus favors faster assembly [*Zhang et al.*, 2009]. As the long-wavelength structure becomes more stable with increasing σ_0, it may also explain the smaller fluctuation than for the weaker plates, with the latter being larger than the average signal. Interestingly, 2-D and 3-D results somewhat deviate from each other in this respect. Although they mostly overlap within the fluctuation margins, the characteristic dispersed interval seems to be elongated for stronger plates in 3-D. This may be a result of the small sample size in 3-D, but it could also reflect the additional complexity, i.e., more directional degrees of freedom for continental drift and the presence of toroidal flow. Both can affect the drift of continents and slow down the assembly.

4. Discussion and Conclusions

The presented calculations suggest that supercontinent formation in a convective system comparable to the Earth's mantle is likely to happen several times from the Archean to present-day. Thus, our models support proposals that the supercontinent cycle is one of Earth's major evolutionary features with all its implications, e.g., thermal insulation [*Brandl et al.*, 2013], modulation of surface heat flow [*Rolf et al.*, 2012], sea level,

climate, and biodiversity [see *Rogers and Santosh*, 2004]. Several previous studies [e.g., *Zhong et al.*, 2007; *Heron and Lowman*, 2011] suggest that supercontinent formation imposes global flow reorganization that finally triggers dispersal and reassembly, such that these processes seem unlikely to occur randomly. Our results suggest that the timescales of reorganization may be controlled by (besides others) the average strength of the lithosphere (Figure 4). However, they also indicate strong time dependence and irregularity imposed by the chaotic nature of mantle convection, which interferes with regularity and enforces severe disturbances in the timing of supercontinent formation. The balance between regular and irregular processes leads to a statistical cyclicity in which the formation of a new supercontinent is roughly guaranteed, but its formation time can only be predicted with a certain probability. The regular formation interval of Earth's past supercontinents as originally proposed by *Worsley et al.* [1984] is included in this statistical cyclicity, but based on our findings, it seems unlikely to be a robust characteristic of the supercontinent cycle.

Our presented models include just the minimum complexity required to study supercontinent dynamics and thus have limitations as discussed earlier. This includes the omission of a stronger lower mantle, which can enforce stabilizing long-wavelength flow [*Bunge et al.*, 1996], although *Zhong et al.* [2007] suggested that a strong lithosphere (as included here) may be equally important for the generation of long-wavelength structures. Also, if more than two continents are considered, collision and breakup events can overlap, which may result in more diffuse timescales [*Condie*, 2011] and even more variation in supercontinent dynamics [*Yoshida and Santosh*, 2014]. Finally, strong plumes possibly disturb continental assembly paths [*Phillips and Bunge*, 2007] and more vigorous mantle flow favors smaller-scale structures as well as faster mixing of subcontinental heat reservoirs [*Heron and Lowman*, 2014], both inducing additional irregularity. Finally, long-term trends like secular cooling and continental growth will add additional time dependence and fluctuation. However, as most of these aspects tend to increase irregularity, the statistical cyclicity as proposed by our basic models is likely to become even more pronounced. Nevertheless, future models need to consider these complexities in order to deepen our understanding of the role of the supercontinent cycle in Earth's evolution.

Acknowledgments

We thank S. Zhong and J. Lowman for their helpful reviews. T.R. thanks F. Capitanio for his support and received funding from Crystal2Plate, a FP-7 funded Marie Curie Action (grant PITN-GA-2008-215353) and the Swiss National Science Foundation (grant 200021-143299). Calculations were performed on ETH's Brutus and on Monte Rosa of the Swiss National Supercomputing Centre (project ID s272). Data available upon request.

The Editor thanks Shijie Zhong and Julian Lowman for their assistance in evaluating this paper.

References

Bradley, D. (2011), Secular trends in the geologic record and the supercontinent cycle, *Earth-Sci. Rev.*, *108*, 16–33.

Brandl, P., M. Regelous, C. Beler, and K. Haase (2013), High mantle temperatures following rifting caused by continental insulation, *Nat. Geosci.*, *6*, 391–394.

Bunge, H.-P., M. A. Richards, and J. R. Baumbartner (1996), Effect of depth-dependent viscosity on the planform of mantle convection, *Nature*, *379*, 436–438.

Campbell, I., and C. Allen (2008), Formation of supercontinents linked to increases in atmospheric oxygen, *Nat. Geosci.*, *1*, 554–558.

Coltice, N., T. Rolf, P. Tackley, and S. Labrosse (2012), Dynamic causes of the relation between area and age of the ocean floor, *Science*, *336*, 335–338.

Condie, K. C., E. Belousova, W. L. Griffin, and K. N. Sircombe (2009), Granitoid events in space and time: Constraints from igneous and detrital zircon age spectra, *Gondwana Res.*, *15*, 228–242.

Condie, K. C. (2011), *Earth as an Evolving Planetary System,* 2nd ed., Elsevier, Amsterdam, Netherlands.

Gurnis, M. (1988), Large-scale mantle convection and the aggregation and dispersal of supercontinents, *Nature*, *332*, 695–699.

Heron, P., and J. Lowman (2011), The effects of supercontinent size and thermal insulation on the formation of mantle plumes, *Tectonophysics*, *510*, 28–38.

Heron, P., and J. Lowman (2014), The impact of Rayleigh number on assessing the significance of supercontinent insulation, *J. Geophys. Res. Solid Earth*, *119*, 711–733, doi:10.1002/2013JB010484.

Lenardic, A., L. Moresi, and H. Mühlhaus (2000), The role of mobile belts for the longevity of deep cratonic lithosphere: The crumple zone model, *Geophys. Res. Lett.*, *27*, 1235–1238.

Meert, J. G. (2012), What's in a name? The Columbia (Paleopangaea/Nuna) supercontinent, *Gondwana Res.*, *21*, 987–993.

Murphy, J., and R. Nance (2003), Do supercontinents introvert or extrovert?: Sm-Nd isotope evidence, *Geology*, *31*, 873–876.

Murphy, J., G. Gutierrez-Alonso, R. Nance, J. Fernandez-Suarez, J. Keppie, C. Quesada, R. Strachan, and J. Dostal (2006), Origin of the Rheic Ocean: Rifting along a Neoproterozoic suture?, *Geology*, *34*, 325–328.

Phillips, B., and H.-P. Bunge (2007), Supercontinent cycles disrupted by strong mantle plumes, *Geology*, *35*(9), 847–850.

Roberts, N. M. W. (2012), Increased loss of continental crust during supercontinent amalgamation, *Gondwana Res.*, *21*, 994–1000.

Rogers, J., and M. Santosh (2003), Supercontinents in Earth history, *Gondwana Res.*, *6*, 357–368.

Rogers, J., and M. Santosh (2004), *Continents and Supercontinents*, Oxford Univ. Press, New York.

Rolf, T., N. Coltice, and P. Tackley (2012), Linking continental drift, plate tectonics and the thermal state of the Earth's mantle, *Earth Planet. Sci. Lett.*, *351-352*, 134–146.

Rolf, T., and P. Tackley (2011), Focussing of stress by continents in 3D spherical mantle convection with self-consistent plate tectonics, *Geophys. Res. Lett.*, *38*, L18301, doi:10.1029/2011GL048677.

Tackley, P., and S. King (2003), Testing the tracer ratio method for modeling active compositional fields in mantle convection simulations, *Geochem. Geophys. Geosyst.*, *4*, 8302, doi:10.1029/2001GC000214.

Turcotte, D., and G. Schubert (2002), *Geodynamics,* 2nd ed., Cambridge Univ. Press, Cambridge, U. K.

Worsley, T., D. Nance, and J. Moody (1984), Global tectonics and eustasy for the past 2 billion years, *Mar. Geol.*, *58*, 373–400.

Xie, S., and P. Tackley (2004), Evolution of U-Pb and Sm-Nd systems in numerical models of mantle convection and plate tectonics, *J. Geophys. Res.*, *109*, B11204, doi:10.1029/2004JB003176.

Yoshida, M. (2008), Mantle convection with longest-wavelength thermal heterogeneity in a 3-D spherical model: Degree one or two?, *Geophys. Res. Lett.*, *35*, L23302, doi:10.1029/2008GL036059.

Yoshida, M., and M. Santosh (2014), Mantle convection modeling of the supercontinent cycle: Introversion, extroversion, or a combination?, *Geosci. Frontiers*, *5*, 77–81.

Zhang, N., S. Zhong, and A. McNamara (2009), Supercontinent formation from stochastic collision and mantle convection models, *Gondwana Res.*, *15*, 267–275.

Zhong, S., N. Zhang, Z. X. Li, and J. H. Roberts (2007), Supercontinent cycles, true polar wander, and very long-wavelength mantle convection, *Earth Planet. Sci. Lett.*, *261*, 551–564.